Combined Mechanical and Circuit Nonlinearities in Electrostatic Vibration Energy Harvesters

Elena Blokhina[1], Danièle Fournier-Prunaret[2], Peter Harte[1], Dimitri Galayko[3] and Orla Feely[1]
[1] University College Dublin, Ireland, [2] LAAS-CNRS, INSA, Toulouse, France, [3] UPMC Sorbonne Universités, Paris, France

***Abstract*—The aim of this paper is to study an electrostatic vibration energy harvester that utilises a nonlinear resonator. A vibration energy harvester represents a system where a mechanical resonator driven by ambient vibrations is coupled with a conditioning electronic circuit, which acts as a damper and converts mechanical energy into electrical. If a nonlinear resonator is embedded into the conditioning circuit, nonlinearity will appear from both mechanical and circuit components of the system. We expand the analytical approach that we developed in our previous works to the case of combined mechanical and circuit nonlinearities. This allow us to analyze steady-state behavior and compare it with the linear case. In addition, we discuss a specific nonlinear phenomena that is introduced by the discontinuity of the system — the sliding bifurcation. We show that the onset of steady-state quasi-harmonic oscillations occur through the disappearance of sliding motion.**

I. Introduction

Vibrational energy harvesters (VEHs) employ high-quality mechanical resonators that can convert vibration energy into electrical. Electrostatic (capacitive) vibration energy harvesters (e-VEHs) convert energy using a capacitive transducer [1], [2]. For a large number of applications, the sources of vibration energy can be described as wideband. Widening of the frequency response of the resonators utilized in VEHs is an important problem and a large number of very recent works propose to employ nonlinear resonators to address this problem [3]–[6].

In our previous works [7]–[10], we presented an analysis of a very common configuration of resonant e-VEHs based on a gap-closing transducer operating in constant-charge mode [1]. Reference [7] proposed a straightforward analytical description of the regular and desirable behaviour of the system. The characteristics of this behaviour can be calculated from parameters of the system and from the environmental parameters (the magnitude and frequency of external vibrations). In addition, [11] highlighted the existence of irregular and undesirable regimes of such e-VEHs, in [8] the quantitative limits of the regular behaviour were identified.

In this work we investigate a VEH consisting of a nonlinear resonator coupled with a conditioning circuit. In this case, nonlinearity appears from both mechanical and circuit components of the system. We show that the theoretical approach from [7] can be successfully applied in this nonlinear case and discuss the differences with the linear case. In addition, we found that the desired quasi-harmonic oscillations appear through a sliding bifurcation and explain this phenomenon in detail.

II. Statement of the problem

A resonant electrostatic VEH consists of a high-Q resonator, a variable capacitor (transducer) C_{tran}, and a conditioning circuit that implements the constant-charge energy conversion cycle [1]. The conditioning circuit discharges the transducer to zero when the transducer capacitance is at a local minimum and charges it to a charge Q_0 when its capacitance is at a local maximum. The energy conversion is achieved when the transducer capacitance decreases keeping its charge Q_0 constant. During this process, mechanical energy is converted into electrical energy, and the transducer acts as a damper in the mechanical domain. A detailed description of the conversion cycle and a schematic view of the system can be found in [9].

In [7], a normalised equation in the form of a nonlinear driven oscillator was obtained to model the system. The normalised displacement y of the resonator is described by

$$y''+2\beta y'+y+\delta y^2+\lambda y^3 = A_{ext}\cos(\Omega\tau+\theta_0)+f_t(y,y') \quad (1)$$

where the prime denotes the derivative with respect to dimensionless time τ. In eq. (1), the force f_t generated by the transducer is piecewise defined. Following [7], we will use the expression $f_t = \nu_0/(1-y_{max})$ if $y' < 0$ and $f_t = 0$ otherwise. Therefore this system is a piecewise smooth dynamical system. It is governed by different vector fields in domains of the state space separated by a switching surface Σ given by the expression $y' = 0$. By introducing the vector of variables $\mathbf{x} = (x_1, x_2, x_3)$ where $x_1 = y$, $x_2 = y'$, $x_3 = \tau$, we can put the system into a normal form $\dot{\mathbf{x}} = \mathbf{F}(\mathbf{x}, \mathbf{P})$, where $\mathbf{P}$ is a vector representing the parameters of the system:

$$\dot{\mathbf{x}} = \begin{cases} \mathbf{F}_1(\mathbf{x},\mathbf{P}), & H(\mathbf{x}) > 0 \\ \mathbf{F}_2(\mathbf{x},\mathbf{P}), & H(\mathbf{x}) < 0 \end{cases} \quad (2)$$

Here the function $H(\mathbf{x}) = -x_2 = 0$ defines the switching surface Σ and the functions $\mathbf{F}_1$ and $\mathbf{F}_2$ are smooth:

$$\mathbf{F}_1 = \begin{pmatrix} x_2 \\ -2\beta x_2 - x_1 - \delta x_1^2 - \lambda x_1^3 + \alpha\cos(\Omega x_3 + \theta_0) + \\ +\frac{\nu_0}{1-x_{1,max}} \\ 1 \end{pmatrix} \quad (3)$$

$$\mathbf{F}_2 = \begin{pmatrix} x_2 \\ -2\beta x_2 - x_1 - \delta x_1^2 - \lambda x_1^3 + \alpha\cos(\Omega x_3 + \theta_0) \\ 1 \end{pmatrix} \quad (4)$$

Note that since $\mathbf{F}_1 \neq \mathbf{F}_2$ on the switching manifold Σ, (2) represents a Filippov system [12].

In the above equations, the following normalised variables were introduced: displacement $y = x/d$ obtained from the dimensional displacement x, time $\tau = \omega_0 t$, dissipation $\beta = b/(2m\omega_0)$, external frequency $\Omega = \omega_{ext}/\omega_0 = 1+\sigma$ where σ is a small mismatch in the two frequencies, $\alpha = A_{ext}/(d\omega_0^2)$, $\nu_0 = W_0/(d^2 m\omega_0^2)$, $\delta = k_2 d/(m\omega_0^2)$ and $\lambda = k_3 d^2/(m\omega_0^2)$. Here m is the mass of the resonator, b is the damping factor, $\omega_0 = \sqrt{k/m}$ is the natural frequency, k is the linear spring

constant, k_2 and k_3 are nonlinear spring constants that stand before the square and the cubic nonlinear terms, d is the rest gap (i.e. the gap in the absence of all forces), A_{ext} is the external acceleration amplitude, ω_{ext} is the external frequency, θ_0 is the initial phase of the external force and W_0 is the energy that the conditioning circuit provides to the transducer at the beginning of each energy conversion cycle (at each local maximum of the transducer capacitance C_{tran} according to the QV cycle implementation, see [9]).

III. Steady-State Theory

In this section we show how to expand the theory developed in [7] to the case of mechanical nonlinearity. The proposed analysis, based on the Multiple Scales Method (MSM), allows one to find steady-state solutions of the original systems. In order to apply this method, we arrange the nonlinear terms in (1) in appropriate order of a small arbitrary parameter ε appearing in the method.

$$y''+2\varepsilon\tilde{\beta}y'+y+\varepsilon\tilde{\delta}y^2+\varepsilon\tilde{\lambda}y^3=\varepsilon\tilde{f}_t(y,y')+\varepsilon\tilde{\alpha}\cos(\tau+\varepsilon\tilde{\sigma}\tau+\theta_0) \tag{5}$$

where the tilde over the parameters denotes the original parameters divided by ε. We assume that the approximation for the solution is $y_{av}+a\cos\theta$ where $\theta=(1+\sigma)\tau+\theta_0$. Now let us use the Fourier series for the nonlinear forces f_t, $\tilde{f}_{sq}(y)=\tilde{\delta}y^2$ and $\tilde{f}_{cb}(y)=\tilde{\lambda}y^3$ restricting ourselves to the case of the first harmonic (due to the high Q of the system).

$$\begin{aligned}\tilde{f}_0(y_{av},a)&=\frac{1}{2\pi}\int_0^{2\pi}\tilde{f}_t(y_0)d\theta=\frac{\nu_0}{2(1-y_{av}-a)}\\ \tilde{a}_1(y_{av},a)&=\frac{1}{\pi}\int_0^{2\pi}\tilde{f}_t(y_0)\cos\theta d\theta=0\\ \tilde{b}_1(y_{av},a)&=\frac{1}{\pi}\int_0^{2\pi}\tilde{f}_t(y_0)\sin\theta d\theta=\frac{2\nu_0}{\pi(1-y_{av}-a)}\end{aligned} \tag{6}$$

and similarly for the quadratic and cubic nonlinear terms

$$\begin{aligned}\tilde{f}_0^{sq}(y_{av},a)&=\frac{1}{2}\tilde{\delta}(a^2+2y_{av}^2)\\ \tilde{a}_1^{sq}(y_{av},a)&=2\tilde{\delta}y_{av}a,\qquad \tilde{b}_1^{sq}(y_{av},a)=0\end{aligned} \tag{7}$$

and

$$\begin{aligned}\tilde{f}_0^{cb}(y_{av},a)&=\frac{1}{2}\tilde{\lambda}(3a^2y_{av}+2y_{av}^3)\\ \tilde{a}_1^{cb}(y_{av},a)&=\frac{3}{4}\tilde{\lambda}(a^3+4ay_{av}^2),\qquad \tilde{b}_1^{cb}(y_{av},a)=0\end{aligned} \tag{8}$$

This means that we have presented nonlinear forces in the form $\tilde{f}=\tilde{f}_0+[\tilde{c}_1e^{i(T_0+\varphi)}]+c.c.$ where $\tilde{c}_1=\tilde{a}_1/2$. Substituting the expansion $y(\tau)=y_0+\varepsilon y_1$ into eq. (5) and following the MSM implementation routine we obtain the equation for the slow complex amplitude $A(T_1)$:

$$\begin{aligned}&-2i\dot{A}e^{iT_0}-2\tilde{\beta}iAe^{iT_0}+\tilde{c}_1(y_{av},a)e^{iT_0+i\varphi}+\tilde{\alpha}/2\times\\ &\times e^{i(T_0+\tilde{\sigma}T_1+\theta_0)}-\tilde{c}_1^{sq}e^{i(T_0+\varphi)}-\tilde{c}_1^{cb}e^{i(T_0+\varphi)}+c.c=0\end{aligned} \tag{9}$$

and

$$y_1=\tilde{f}_0-\tilde{f}_0^{sq}-\tilde{f}_0^{cb} \tag{10}$$

or $y_{av}=\varepsilon(\tilde{f}_0-\tilde{f}_0^{sq}-\tilde{f}_0^{cb})$. Dividing (9) into real and imaginary parts will give equations for the slow real amplitude a and the phase $\psi=\tilde{\sigma}T_1+\theta_0-\varphi$. The steady-state solution a_0 and ψ_0 are found from the condition $\dot{a}=0$ and $\dot{\psi}=0$. For the phase ψ_0 one obtains a set of equations (assuming only nonzero harmonic coefficients)

$$\begin{aligned}\frac{\tilde{\alpha}}{2}\sin\psi_0&=\tilde{\beta}a_0+\frac{\tilde{b}_1(y_{av,0},a_0)}{2},\\ \frac{\tilde{\alpha}}{2}\cos\psi_0&=-a_0\tilde{\sigma}+\frac{\tilde{a}_1^{sq}(y_{av,0},a_0)}{2}+\frac{\tilde{a}_1^{cb}(y_{av,0},a_0)}{2}\end{aligned} \tag{11}$$

The equation for the amplitude a_0 can now be found from (11)

$$\begin{aligned}\frac{\tilde{\alpha}^2}{4}=&\left(\tilde{\beta}a_0+\frac{\tilde{b}_1(y_{av,0},a_0)}{2}\right)^2+\\ &\left(a_0\tilde{\sigma}-\frac{\tilde{a}_1^{sq}(y_{av,0},a_0)}{2}-\frac{\tilde{a}_1^{cb}(y_{av,0},a_0)}{2}\right)^2\end{aligned} \tag{12}$$

The necessary stability analysis is based on calculating the eigenvalues of the Jacobian of the system that describes the evolution of small perturbations from the steady-state a_0 and ψ_0 in time [8].

Using the steady-state theory, we can calculate the oscillation envelope (i.e. its minimum and maximum values $y_{max}=y_{av,0}+a_0$ and $y_{min}=y_{av,0}-a_0$) as a function of the control parameters. Examples of the envelopes of oscillations as a function of the transducer parameter W_0 at three different external accelerations A_{ext} are shown in

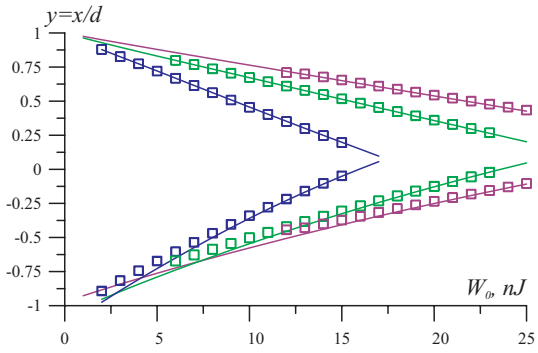

Fig. 1. Steady-state theory versus numerical simulations: the envelope of oscillations y_{max} and y_{min} as a function of the energy W_0 at three different external acceleration amplitudes $A_{ext}=3$, 5 and 7 m/s^2 (the blue, green and purple lines correspondingly). Steady-state oscillations envelopes found from numerical simulations are shown by the squares. Nonlinearity parameters $\delta=0.3$ and $\lambda=0.2$, the frequency mismatch $\sigma=0.04$.

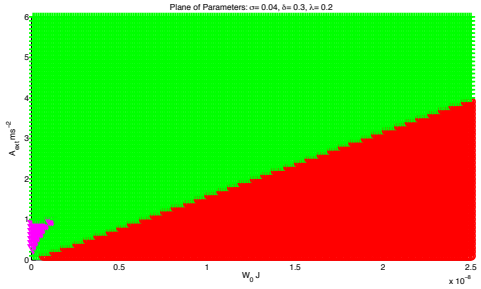

Fig. 2. Steady-state theory: plane of parameters (W_0, A_{ext}) where the area of no oscillations is denoted by red, the area of multistabilty is denoted by purple and of single steady-state solutions is denoted by green. Other parameters are $\delta=0.3$, $\lambda=0.2$, $\sigma=0.04$.

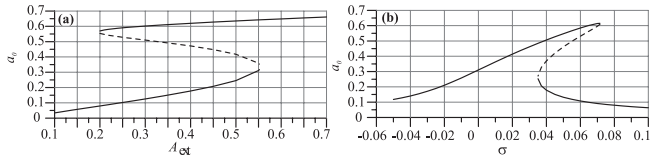

Fig. 3. Steady-state theory: coexisting oscillations. (a) The amplitude of oscillations versus the parameter A_{ext} at $W_0 = 0.3\ nJ$, $\sigma = -0.04$, $\delta = 0.3$ and $\lambda = -0.3$. and (b) the amplitude of oscillations versus the parameter σ (or dimensionless frequency) at $W_0 = 0.7\ nJ$, $A_{ext} = 0.4\ m/s^2$, $\delta = 0.01$ and $\lambda = 0.5$. Stable branches are shown by solid lines and unstable by dashed lines.

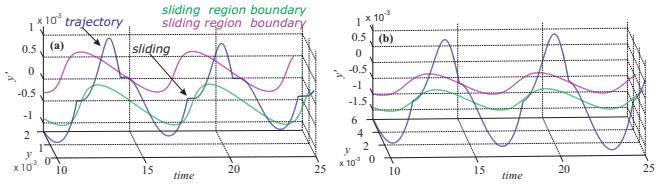

Fig. 4. The state space: (a) — a trajectory (blue) displays sliding motion when it crosses the switching surface in the sliding region bounded by Σ^+ and Σ^- (shown by green and purple). $A_{ext} = 0.0489\ m/s^2$. (b) — sliding bifurcation: the trajectory crosses the switching surface through the sliding region boundaries. $A_{ext} = 0.046\ m/s^2$. Other parameters: $W_0 = 0.3\ nJ$, $\delta = 0.3$, $\lambda = 0.2$, $\sigma = 0.3$.

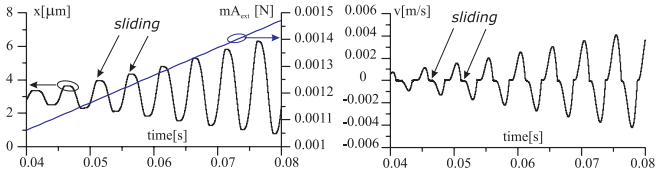

Fig. 5. VHDL–AMS modeling of the sliding bifurcation: evolution of the displacement $x(t)$ and the velocity $v(t)$ with time at a slow change of acceleration A_{ext}. Other parameters: $W_0 = 30\ nJ$, $\delta = \lambda = 0$ (the linear case), $\sigma = 0.3$.

Fig. 1. For comparison, steady-state oscillations calculated numerically by simulating (2) are shown by the squares. In the original nonlinear system, steady-state oscillations exist for a limited range of W_0 and A_{ext}: as we show in [8], the behavior of the system is more complex and it can display bifurcations and irregular oscillations. Note that the nonlinearity parameters $\delta = 0.3$ and $\lambda = 0.2$ are deliberately chosen to be rather large since it allows us to point out the effects caused by mechanical nonlinearity (estimations based on [6] give realistic values as $\delta,\ \lambda \lesssim 0.1$).

Mechanical nonlinearity causes this system to be multistable (i.e. two or more stable solutions exist in the system) at certain values of the control parameters. In contrast to a linear resonator with the gap-closing transducer considered in [7] (where only one solution $y_{max} < 1$ exists), nonlinearity allows the system to have two stable physical solutions at small energies and accelerations. Figure 2 shows the plane (W_0, A_{ext}) where we denote the area of no oscillations, multistability and of a single steady-state solution.

The evolution of the coexisting oscillations versus a selected parameter (a bifurcation diagram) is shown in fig 3. If one traces the evolution of the amplitude of oscillation as a function of the normalized frequency mismatch σ, one obtains a well-known hysteresis frequency response typical for nonlinear driven oscillators (Fig. 3b).

IV. Sliding Bifurcation

The sliding bifurcation is a discontinuity induced bifurcation that can occur in Filippov systems. In the state space of such systems, there can exist a so-called sliding region $\hat{\Sigma}$ that belongs to the switching surface (or manifold) Σ. The sliding region is an area such that trajectories coming to it move tangentially until they reach the boundary of the region. The sliding bifurcation describes the critical case when a trajectory crossing the switching surface, passes exactly through one of the boundaries of the sliding region. A small perturbation of such a trajectory will generate either a non-sliding trajectory (passes Σ transversally) or a trajectory with sliding (contains a piece of trajectory with tangential motion along the sliding region $\hat{\Sigma}$). As we shall see from this section, a sliding mode precedes the onset of harmonic oscillations and it is undesired behavior that limits the performance of the device.

Firstly, we note that the approach we develop based on the MSM allows one to find the necessary conditions to start oscillations. This condition determines the moment when a positive nonzero amplitude of oscillations a_0 appears. This condition is given by two the expressions (10) and (11) taken at the condition that $a_0 = 0$ and solved with respect to $y_{av,0}$ and one of the control parameters ν_0 (dimensionless version of W_0) or α (dimensionless version of A_{extn}). Below these values the systems display irregular very small scale movements, and only above this condition are harmonic oscillations possible. Immediately after the condition is fulfilled, one observes periodic orbits that contain the intervals of sliding motion. Only after the sliding bifurcation the desired harmonic oscillations appear. This is clearly a parasitic phenomenon since this system operates effectively only when one maximum is detected per one cycle of oscillations. In the sliding mode, the conditioning circuit will detect a large number of local extrema since the sliding takes place on the surface $y' = 0$. Therefore, this will make the conditioning circuit operate ineffectively.

Now we define the switching surface (manifold) as $\Sigma = \left\{\mathbf{x} \in \mathbf{R}^3 / H(\mathbf{x}) = 0\right\}$. The normal vector to this surface is $\mathbf{n} = \nabla H = [0,\ -1,\ 0]$. According to [13], the following condition holds throughout the sliding region: $\langle \nabla H, \mathbf{F}_2 \rangle - \langle \nabla H, \mathbf{F}_1 \rangle > 0$. Here $\langle \mathbf{a}, \mathbf{b} \rangle$ denotes the inner product of two vectors. Note that this condition is always fulfilled since $\langle \nabla H, \mathbf{F}_2 \rangle - \langle \nabla H, \mathbf{F}_1 \rangle = \frac{\nu_0}{1 - y_{max}}$. Let us define the vector field $\mathbf{F}_s$ that governs the sliding flow inside the switching region [13].

$$\mathbf{F}_s = \tfrac{\mathbf{F}_1 + \mathbf{F}_2}{2} + \rho(\mathbf{x}) \tfrac{\mathbf{F}_2 - \mathbf{F}_1}{2} \left(= \mathbf{F}_1 \tfrac{1-\rho}{2} + \mathbf{F}_2 \tfrac{1+\rho}{2}\right) \qquad (13)$$

where $|\rho| \leq 1$. The function ρ can be obtained by considering that $\mathbf{F}_s$ must be tangential to the switching manifold Σ, i.e., $\langle \nabla H, \mathbf{F}_s \rangle = 0$. We obtain:

$$\rho(\mathbf{x}) = -\tfrac{\langle \nabla H, \mathbf{F}_2 \rangle + \langle \nabla H, \mathbf{F}_1 \rangle}{\langle \nabla H, \mathbf{F}_2 \rangle - \langle \nabla H, \mathbf{F}_1 \rangle} \qquad (14)$$

Let us define the sliding region $\hat{\Sigma} = \{\mathbf{x} \in \Sigma / |\rho(\mathbf{x})| < 1\}$ and its boundaries:

$$\partial\hat{\Sigma}^- = \{\mathbf{x} \in \Sigma / \rho(\mathbf{x}) = -1\}, \partial\hat{\Sigma}^+ = \{\mathbf{x} \in \Sigma / \rho(\mathbf{x}) = +1\} \qquad (15)$$

If the intersection of a trajectory with the sliding region boundaries takes place at $\mathbf{x} = \mathbf{x}^\star$, the following conditions define the bifurcation scenario [12]:

$$H(\mathbf{x}^\star) = 0, \qquad \nabla H(\mathbf{x}^\star) \neq 0 \tag{16a}$$

$$\rho(\mathbf{x}^\star) = -1 \Leftrightarrow \mathbf{F}_s = \mathbf{F}_1 \Leftrightarrow \langle \nabla H, \mathbf{F}_1 \rangle|_{\mathbf{x}=\mathbf{x}^\star} = 0 \tag{16b}$$

$$\rho(\mathbf{x}^\star) = +1 \Leftrightarrow \mathbf{F}_s = \mathbf{F}_2 \Leftrightarrow \langle \nabla H, \mathbf{F}_2 \rangle|_{\mathbf{x}=\mathbf{x}^\star} = 0 \tag{16c}$$

$$\text{Sliding type I: } \left\langle \nabla H, \frac{\partial \mathbf{F}_1}{\partial x}\mathbf{F}_1 \right\rangle > 0 \tag{16d}$$

$$\text{Sliding type II: } \left\langle \nabla H, \frac{\partial \mathbf{F}_1}{\partial x}\mathbf{F}_1 \right\rangle < 0 \tag{16e}$$

In our case, the condition (16a) is verified. When $H(\mathbf{x}) = -x_2 = 0$ we can write that $x_1 = y_{max}$ (on condition that $x_2' = y'' < 0$). Assuming that $\theta_0 = 0$ (or it is eliminated by a simple transformation of variables), expressions (16b) and (16c) turn into:

$$\rho(\mathbf{x}^\star) = +1 : \ \lambda x_1^3 + \delta x_1^2 + x_1 - \alpha\cos(\Omega x_3) = 0 \tag{17a}$$

$$\rho(\mathbf{x}^\star) = -1 : \ \lambda x_1^4 + (\delta - \lambda)x_1^3 + (1-\delta)x_1^2 - \tag{17b}$$
$$- (1 + \alpha\cos(\Omega x_3))x_1 + \nu_0 + \alpha\cos(\Omega x_3) = 0$$

Equation (17a) is solved using Cardano's method and equation (17b) is solved using Ferrari's method. As a result we obtain a set of analytically obtained expressions that define the sliding region boundaries in the state space. Now system (2) can be evaluated in time together with Σ^+ and Σ^- and one can determine at which parameters a sliding mode appears or disappears.

An example of a sliding mode is shown in Fig. 4a. Sliding is displayed if a trajectory, while crossing the switching surface Σ, hits the sliding region $\hat{\Sigma}$. Varying one of the control parameters, A_{ext} in our case, we can see that the trajectory crosses Σ and passes it exactly at the boundaries Σ^+ and Σ^- (Fig. 4b). Further small increase of A_{ext} will result in a non-sliding trajectory. Note that in this system the sliding mode always precedes the onset of desired harmonic oscillations. Sliding motion was also found in mixed signal simulations that is known as a powerful to for the analysis of nonlinear circuits and systems. In this work we use a VHDL-AMS model developed in [7], [11]). The waveforms of the displacement $x(t)$ and the velocity $v(t)$ with characteristic 'plateaus' at the switching surface area shown in Fig. 5. As the bifurcation parameter A_{ext} increases, the transition from sliding motion to non-sliding oscillations is visible.

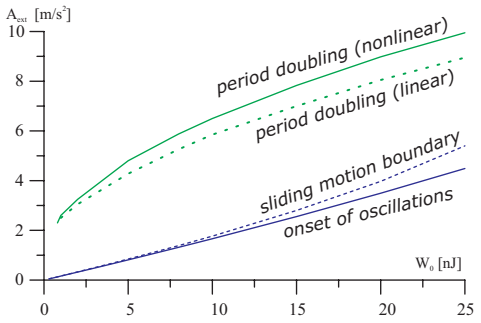

Fig. 6. Plane of parameters (W_0, A_{ext}) where the starting condition is shown by the blue line, the sliding bifurcation line is shown by dashed blue, the period doubling bifurcation is shown by green. For comparison, the period doubling bifurcation in the case of the linear resonator ($\lambda = \delta = 0$) is shown by the dashed green line. For parameters, see Fig. 4.

Finally we note that, similarly to the linear case, the period doubling bifurcation is another phenomenon that limits the region of harmonic oscillations in the system [8]. Nonlinearity slightly changes the bifurcation values of parameters W_0 and A_{ext} (two bifurcation lines, one for the linear system with $\delta = \lambda = 0$ and the other for the nonlinear system are shown in Fig. 6).

V. Conclusions

We have studied an electrostatic vibration energy harvester with a nonlinear resonator. In this case, nonlinearity appears from both mechanical and electronic components of the system. We applied a perturbation method to find steady-state characteristics of the system and compared them with the linear case. In general, we conclude that the steady-state theory developed in our previous works describes nonlinear systems very well. We have found that for the systems with mechanical nonlinearity, there exists a region of multistability. In addition, we discuss the sliding bifurcation, a nonlinear phenomena that is introduced by discontinuity of the system. The sliding mode is a parasitic effect and always precedes the onset of stable harmonic oscillations in this type of systems. The sliding bifurcation is also verified by mixed signal VHDL–AMS modeling.

References

[1] S. Meninger, J. Mur-Miranda, R. Amirtharajah, A. Chandrakasan, and J. Lang, "Vibration-to-electric energy conversion," *Very Large Scale Integration (VLSI) Systems, IEEE Transactions on*, vol. 9, no. 1, pp. 64–76, 2001.

[2] P. Mitcheson, E. Yeatman, G. Rao, A. Holmes, and T. Green, "Energy harvesting from human and machine motion for wireless electronic devices," *Proceedings of the IEEE*, vol. 96, no. 9, pp. 1457–1486, 2008.

[3] S. D. Nguyen and E. Halvorsen, "Nonlinear springs for bandwidth-tolerant vibration energy harvesting," *J. Microelectromech. Syst.*, vol. 20, pp. 1225–1227, 2011.

[4] D. A. W. Barton, S. G. Burrow, and L. R. Clare, "Energy harvesting from vibrations with a nonlinear oscillator," *J. Vib. Acoust.*, vol. 132, pp. 0 210 091–0 210 097, 2012.

[5] B. Andò, S. Baglio, C. Trigona, N. Dumas, L. Latorre, and P. Nouet, "Nonlinear mechanism in mems devices for energy harvesting applications," *Journal of Micromechanics and Microengineering*, vol. 20, p. 125020, 2010.

[6] M. Amri, P. Basset, F. Cottone, D. Galayko, F. Najar, and T. Bourouina, "Novel nonlinear spring design for wideband vibration energy harvesters," in *PowerMEMS*, 2011.

[7] E. Blokhina, D. Galayko, P. Basset, and O. Feely, "Steady-state oscillations in resonant electrostatic vibration energy harvesters," *IEEE Trans. Circuits Syst. I*, p. (in press), 2013.

[8] E. Blokhina, D. Galayko, R. Wade, P. Basset, and O. Feely, "Bifurcations and chaos in electrostatic vibration energy harvesters," in *IEEE International Symposium on Circuits and Systems 2012, Seoul, Korea, 20 – 24 May 2012*, 2012, pp. 397–400.

[9] D. Galayko and P. Basset, "A general analytical tool for the design of vibration energy harvesters (VEHs) based on the mechanical impedance concept," *IEEE Trans. Circuits Syst. I*, no. 99, pp. 299–311, 2011.

[10] E. Blokhina, D. Galayko, P. Harte, P. Basset, and O. Feely, "Limit on converted power in resonant electrostatic vibration energy harvesters," *Appl. Phys. Lett.*, vol. 101, p. 173904, 2012.

[11] D. Galayko, R. Guillemet, A. Dudka, and P. Basset, "Comprehensive dynamic and stability analysis of electrostatic vibration energy harvester (E-VEH)," in *2011 International Conference on Solid-State Sensors, Actuators and Microsystems (TRANSDUCERS)*, 2011, pp. 2382–2385.

[12] M. di Bernardo, C. J. Budd, A. R. Champneys, and P. Kowalczyk, *Piecewise-Smooth Dynamical Systems: Theory and Applications*. Springer-Verlag, 2008.

[13] M. di Bernardo, P. Kowalczyk, and A. Nordmark, "Sliding bifurcations: A novel mechanism for the sudden onset of chaos in dry friction oscillators," *Int J. Bifurcation and Chaos*, vol. 276, pp. 121–139, 2003.